

# Calcium Ion Permeation through the Calcium Release Channel (Ryanodine Receptor) of Cardiac Muscle

Duan P. Chen<sup>\*,†</sup>

Department of Molecular Biophysics & Physiology, Rush Medical College, Chicago, Illinois 60612

Le Xu<sup>†</sup>

Department of Biochemistry & Biophysics, University of North Carolina, Chapel Hill, North Carolina 27599

Bob Eisenberg

Department of Molecular Biophysics & Physiology, Rush Medical College, Chicago, Illinois 60612

Gerhard Meissner

Department of Biochemistry & Biophysics, University of North Carolina, Chapel Hill, North Carolina 27599

Received: May 22, 2003; In Final Form: June 18, 2003

Single-channel current–voltage (IV) relations were measured from the calcium release channel of cardiac sarcoplasmic reticulum (RyR2) in 21 mixed solutions of 250 mM alkali metal ions (Na<sup>+</sup>, K<sup>+</sup>, and Cs<sup>+</sup>) with sarcoplasmic reticulum luminal Ca<sup>++</sup> ranging from 5 to 50 mM and Mg<sup>++</sup> from 1 to 50 mM. The measured IV relations were analyzed by the extended Poisson–Nernst–Planck (PNP) formulation (Chen, D. P.; Xu, L.; Tripathy, A.; Meissner, G.; Eisenberg, B. *Biophys. J.* **1999**, *76*, 1346) to give the permeation properties of Ca<sup>++</sup> and Mg<sup>++</sup>. The results indicate that applying PNP theory, two adjustable parameters (diffusion coefficient (*D*) and “excess” chemical potentials ( $\bar{\mu}$ )) suffice to predict the flow of Ca<sup>++</sup> from the sarcoplasmic reticulum in cardiac muscle. The fitting parameters for Ca<sup>++</sup> and Mg<sup>++</sup> are  $D(\text{Ca}) = 8.4 \pm 0.7 \times 10^{-8} \text{ cm}^2/\text{s}$ ,  $\bar{\mu}(\text{Ca}) = -91 \pm 6 \text{ mV}$  and  $D(\text{Mg}) = 5.4 \pm 0.7 \times 10^{-8} \text{ cm}^2/\text{s}$  and  $\bar{\mu}(\text{Mg}) = -53 \pm 6 \text{ mV}$ . The data are used to predict the calcium ion activity profiles in the RyR2 pore, the calcium ion fluxes in solutions of physiological interest, and the competitive permeation of Ca<sup>++</sup> and Mg<sup>++</sup>.

## Introduction

Ryanodine receptors (RyRs) are Ca<sup>++</sup> channels that control cellular functions by releasing Ca<sup>++</sup> from the sarco/endoplasmic reticulum. In mammalian cells, three structurally and functionally related RyR isoforms are RyR1 predominant in skeletal muscle, RyR2 predominant in cardiac muscle, and RyR3 that was initially isolated from brain but is found in many tissues.<sup>2–4</sup> The RyRs have been isolated as 30S protein complexes composed of four large subunits with a molecular mass of 560 kDa and four associated small 12 kDa FK506 binding proteins (FKBP). Negative staining, cryo-electron microscopy, and image analysis show that the RyRs are made up of a large, loosely packed 29 × 29 × 12 nm cytosolic foot region and a smaller transmembrane region that extends ~7 nm toward the SR lumen.<sup>5</sup> Four<sup>6</sup> to as many as 12<sup>7</sup> membrane-spanning segments in the C-terminal region have been predicted to form the Ca<sup>++</sup>-channel pore region of RyRs. The four-membrane-spanning segment model is supported by studies with SR luminal site-directed antibodies<sup>8</sup> and single-channel recordings with tryptic fragments<sup>9</sup> and by studies with deletion mutants.<sup>10</sup> The remaining amino acids of the RyRs form the large catalytic cytoplasmic foot structure.

The RyR channels are regulated by cytosolic Ca<sup>++</sup> and SR luminal Ca<sup>++</sup>. They are activated by the binding of Ca<sup>++</sup> at cytosolic high-affinity sites and are inhibited by the binding of Ca<sup>++</sup> at low-affinity sites. SR luminal Ca<sup>++</sup> has been reported to regulate directly the skeletal and cardiac muscle RyRs by binding to luminal Ca<sup>++</sup> sensing channel sites<sup>11,12</sup> or indirectly by accessing cytosolic Ca<sup>++</sup> activation and inactivation sites following passage through the channel.<sup>13,14</sup>

RyR ion channels are cation-selective channels that display a high ion conductance for monovalent cations (~750 pS with 250 mM K<sup>+</sup> as the current carrier) and divalent cations (~150 pS with 50 mM Ca<sup>++</sup>). The existence of a large Ca<sup>++</sup> conductance was originally demonstrated in single-channel recordings with native skeletal and cardiac muscle SR vesicles fused with planar lipid bilayers,<sup>15,16</sup> and subsequently in studies with purified RyRs incorporated in lipid bilayers.<sup>17,18</sup> RyRs have a broad selectivity for monovalent cations with permeability ratios close to 1 for K<sup>+</sup> relative to Li<sup>+</sup> and Na<sup>+</sup>.<sup>1,18,19</sup> Although RyRs have a higher ion conductance for monovalent cations than Ca<sup>++</sup>, they are selectively permeable for Ca<sup>++</sup> with permeability ratios of 5–7 for Ca<sup>++</sup> relative to K<sup>+</sup> and Na<sup>+</sup>.<sup>18,20,21</sup>

Two models have been described to calculate individual ion fluxes through RyRs in mixed solutions. Tinker et al.<sup>21</sup> developed a barrier model that consists of four barriers and three

\* Corresponding author. E-mail: dchen@rush.edu. Tel: 312-942-5312. Fax: 312-942-6425.

<sup>†</sup> These authors contributed equally to this work.

wells (binding steps) to describe the ionic conductance of the cardiac RyR with both monovalent and divalent cations as permeant species. A limitation of the barrier model is that the data cannot be fitted at high applied transmembrane potentials, even if a prefactor appropriate for the gas phase is used. An increase in the number of barriers (peaks and wells) improved the fits; however, it also required the introduction of a large number of free parameters. The flow of monovalent cations through the cardiac RyR has been also modeled using an extension of the Poisson–Nernst–Planck formulation of electrodiffusion.<sup>1,22</sup> The theory fits all the data over a wide range of applied voltages with the following few adjustable parameters: the diffusion coefficient of each ion species, an average effective charge distribution on the wall of the pore, and an offset in chemical potential which describes the chemical interaction of the cations with the pore wall. This offset in chemical potential reflects the energy difference for an ion in bulk and in the channel pore environment. Using the fitted values of excess chemical potential and the fixed charge distribution, the theory predicts a high alkali metal ion concentration ( $\sim 4$  M) in the channel filter (7 Å diameter, 10 Å long) at bath concentrations as low as 25 mM, and thereby offers an explanation for the high monovalent cation conductances of the RyRs. The theory also explains the discrepancy between “selectivities” defined by conductance sequence and selectivities determined by the permeability ratios (i.e., reversal potentials) in bi-ionic conditions. Conductance selectivity arises mostly from friction: different species of ions have different diffusion coefficients in the channel. Permeability selectivity of an ion is determined by its electrochemical potential gradient and local chemical interaction with the channel. The extended PNP formulation offers a successful combined treatment of selectivity and permeation.

In the present study, we extend the PNP theory to mixed ionic solutions containing  $\text{Ca}^{++}$  and  $\text{Mg}^{++}$ . The current–voltage relationships of single cardiac RyRs were determined in solutions of  $\text{Ca}^{++}$ ,  $\text{Mg}^{++}$ , and monovalent cations and fitted by an extension of the Poisson–Nernst–Planck formulation of electrodiffusion. The results indicate that the PNP theory requires only two adjustable parameters to predict the flow of  $\text{Ca}^{++}$  from the sarcoplasmic reticulum. We thus provide a simple model for future studies of the  $\text{Ca}^{++}$  conductance of the RyRs and other channels.

## Materials and Methods

**Lipid Bilayer Recordings.** Single-channel measurements were performed by fusing proteoliposomes containing purified cardiac RyR with Mueller-Rudin type bilayers containing phosphatidylethanolamine, phosphatidylserine, and phosphatidylcholine in the ratio 5:3:2 (25 mg of total phospholipid per mL *n*-decane).<sup>23</sup> The two sides of the bilayer are defined as cis (cytosolic) and trans (SR lumenal), and the trans side is electrically grounded. Unless otherwise indicated, single channels were recorded in solutions of 0.25 M NaCl, 0.25 M KCl, or 0.25 M CsCl (with 2 mM KHepes at pH 7.5) containing 4  $\mu\text{M}$   $\text{Ca}^{++}$  on the cis side to activate the channels. Different  $\text{CaCl}_2$  from 4  $\mu\text{M}$  to 50 mM were added to the trans side. The ionic solutions used for measuring IV curves and obtaining extended PNP parameters are listed in Tables 1 and 2. Electrical signals were filtered at 0.5 or 2 kHz, digitized at 10 kHz, and analyzed by pClamp software (Axon Instruments).

**Data Analysis.** Analysis of the permeation data of mono- and divalent cations through the RyR2 by the extended PNP

**TABLE 1: The Fifteen Solutions of Mixture of Monovalent Alkaline Metal Ions With Calcium Ions<sup>a</sup>**

cis side		trans side	
XCl	$\text{CaCl}_2$	XCl	$\text{CaCl}_2$
250 mM	4 $\mu\text{M}$	250 mM	4 $\mu\text{M}$
250 mM	4 $\mu\text{M}$	250 mM	5 mM
250 mM	4 $\mu\text{M}$	250 mM	10 mM
250 mM	4 $\mu\text{M}$	250 mM	50 mM
250 mM	4 $\mu\text{M}$	0	25 mM

<sup>a</sup> X stands for Na, K, or Cs.

**TABLE 2: The Ionic Solutions of Mixture of  $\text{K}^+$ ,  $\text{Mg}^{++}$ , and  $\text{Ca}^{++}$**

cis side			trans side		
KCl	$\text{MgCl}_2$	$\text{CaCl}_2$	KCl	$\text{MgCl}_2$	$\text{CaCl}_2$
250 mM	0	4 $\mu\text{M}$	250 mM	5 mM	4 $\mu\text{M}$
250 mM	0	4 $\mu\text{M}$	250 mM	10 mM	4 $\mu\text{M}$
250 mM	0	4 $\mu\text{M}$	250 mM	50 mM	4 $\mu\text{M}$
250 mM	0	4 $\mu\text{M}$	0	25 mM	4 $\mu\text{M}$
125 mM	1 mM	4 $\mu\text{M}$	125 mM	1 mM	4 $\mu\text{M}$
125 mM	1 mM	4 $\mu\text{M}$	125 mM	1 mM	2 mM

formulation was performed as described.<sup>1,24</sup> In the extended PNP formulation, the chemical potential of an ion is given by

$$\mu_j = k_B T \ln C_j + z_j e \Psi + \bar{\mu}_j \quad (1)$$

In addition to the concentration and electrical potential terms that are described by the Poisson–Nernst equation, an “excess” chemical potential ( $\bar{\mu}_j$ ) is added. The excess chemical potential ( $\bar{\mu}_j$ ) represents the free energy needed for an ion to occupy a space in the restricted environment of the channel’s pore, and it describes the intrinsic local chemical interactions of an ion with its environment, in addition to the electrostatic interaction. The extended PNP formulation reads after substituting the above definition of chemical potential into the flux formula:<sup>1,24</sup>

$$-\epsilon_a \Psi''(z) = \frac{2\epsilon_m}{R^2 \ln R/L} [(1 - z/L)\Delta + \Psi(z) - \Psi_{\text{bi}}(L)] + \sum_j z_j e C_j(z) + P(z) \quad (2)$$

$$J_j = -D_j \frac{d\mu_j}{dz} \quad (3)$$

$$= -D_j \left[ \frac{dC_j(z)}{dz} + z_j \frac{e}{k_B T} C_j(z) \frac{d\Psi(z)}{dz} + \frac{C_j(z)}{k_B T} \frac{d\bar{\mu}_j}{dz} \right], \quad \text{for } j = 1 \dots N$$

with boundary conditions

$$\Psi(0) = \Psi_{\text{bi}}(0) + V_{\text{appl}} \quad (4)$$

$$\Psi(L) = \Psi_{\text{bi}}(L) \quad (5)$$

$$C_j(0) = C_j(l) e^{-z_j e \Psi_{\text{bi}}(0)/k_B T}, \quad \text{for } j = 1 \dots N, \quad \text{at } z = 0 \quad (6)$$

$$C_j(L) = C_j(r) e^{-z_j e \Psi_{\text{bi}}(L)/k_B T}, \quad \text{for } j = 1 \dots N, \quad \text{at } z = L \quad (7)$$

where  $L$  is the length of the channel,  $R$  is the radius,  $P(z)$  is the charge distribution of the channel protein defined in the domain  $[0, L]$ ,  $C_j(l)$  is the concentration in the left bath and  $C_j(r)$  the concentration in the right bath,  $\epsilon_a$  is the dielectric constant of the aqueous pore,  $\epsilon_m$  is the dielectric constant of the channel protein and the lipid membrane,  $V_{\text{appl}}$  is the applied voltage,

$\Delta = V_{\text{appl}} + \Psi_{\text{bi}}(0) - \Psi_{\text{bi}}(L)$ , and  $\Psi_{\text{bi}}$  is the usual Donnan potential.<sup>25–27</sup>  $\bar{\mu}_j$  is the excess chemical potential, and the subscript  $j$  denotes the ion species. The electric current is then  $I = A \sum_j z_j J_j$ , where  $A$  is the channel cross sectional area.

In eq 2, the first term on the right-hand side is a dielectric polarization charge. The second term is the charge carried by the mobile ions, and the third term is the charge on the channel protein. The first two terms in the extended flux formula (see eq 3) are the usual flux components from the concentration gradient and another component of flux driven by electric field. The extension is in the third term, which originates from the gradient of the excess chemical potential due to a different local chemical interaction. The above coupled equations are solved numerically, and the procedure to solve the above equations has been described.<sup>1</sup>

In the calculation, the bath concentrations in eqs 6 and 7 are replaced with activities. The activity  $a$  is defined as

$$a = \gamma C$$

where  $C$  is the ionic concentration and  $\gamma$  is the activity coefficient. The activity coefficient in the baths is taken from Table 19 of ref 28, and assumed to be 1 inside the RyR2 selectivity filter (i.e.,  $C = a$ ). Once the concentrations are replaced with the activities in the boundary conditions (at the two openings of the channel), the concentration inside the pore is found by integrating eq 3.

In the extended PNP theory, the channel protein and lipid membrane are described as dielectric media ( $\epsilon_m$ ) with a fixed charge distribution,  $P(z)$ . Each ion species is described by three parameters: valence ( $z_j$ ), diffusion coefficient ( $D_j$ ), and the excess chemical potential ( $\bar{\mu}_j$ ). In the calculation, the function form of the excess chemical potential is simply assumed to be a step function, with different value in the baths than in the pore. It has been shown<sup>1</sup> that the exact smoothing of the discontinuity of the excess chemical potential is not critical, and it will only perturb the numerical value a little.

To predict the calcium ion conductance in solutions containing  $\text{Ca}^{++}$  ions as conducting ions, the diffusion coefficient and the excess chemical potential of  $\text{Ca}^{++}$  are needed as described above, because they are the input parameters to the extended PNP theory. The permeation parameters of  $\text{Ca}^{++}$  ions can be obtained by a least-squares fit of the extended PNP theory to the single-channel current–voltage relations in mixtures of monovalent salts with  $\text{Ca}^{++}$ . The measured single-channel current–voltage relations, in solutions listed in Table 1, are fitted by the extended PNP formulation to obtain (extract) the permeation properties of  $\text{Ca}^{++}$ . All the other parameters in the extended PNP theory, except those of  $\text{Ca}^{++}$ , are taken from the literature.<sup>1</sup> The literature values were not adjusted to improve the fit. Specifically, the geometry of the selectivity filter is  $R = 3.5 \text{ \AA}$ ,  $L = 10 \text{ \AA}$ , and the dielectric property is defined by  $\epsilon_m = 2$ ,  $\epsilon_a = 80$ . The average charge distribution along the filter region is  $P(z) = -4.1(\pm 0.2)\text{M}$ . The parameters of monovalent cations ( $\text{Na}^+$ ,  $\text{K}^+$ , and  $\text{Cs}^+$ ) are taken (again as they are without change) from Table 3 of ref 1, and they are as follows:  $D(\text{Na}) = 7.8(\pm 0.9) \times 10^{-7} \text{ cm}^2/\text{s}$ ,  $\bar{\mu}(\text{Na}) = -25(\pm 2) \text{ mV}$ ;  $D(\text{K}) = 1.3(\pm 0.2) \times 10^{-6}$ ,  $\bar{\mu}(\text{K}) = 0 \text{ mV}$ ;  $D(\text{Cs}) = 8.3(\pm 0.8) \times 10^{-7}$ ,  $\bar{\mu}(\text{Cs}) = 1.3(\pm 0.1) \text{ mV}$ ; and  $D(\text{Cl}) < 4.1 \times 10^{-6}$ ,  $\bar{\mu}(\text{Cl}) = 0 \text{ mV}$ .  $D(\text{Cl})$  is set to  $4.1 \times 10^{-9}$  in the calculation, but it can be set to a value up to  $4.1 \times 10^{-6}$  without affecting the numerical result significantly. Once the diffusion coefficient and excess chemical potential of  $\text{Ca}^{++}$  are obtained by the least-squares fit (using the experimentally measured IV's in the salt solutions of monovalent cations with  $4 \mu\text{M}$  cis  $\text{Ca}^{++}$ ), the single-channel

## PNP fit to the RyR2 IV Relations

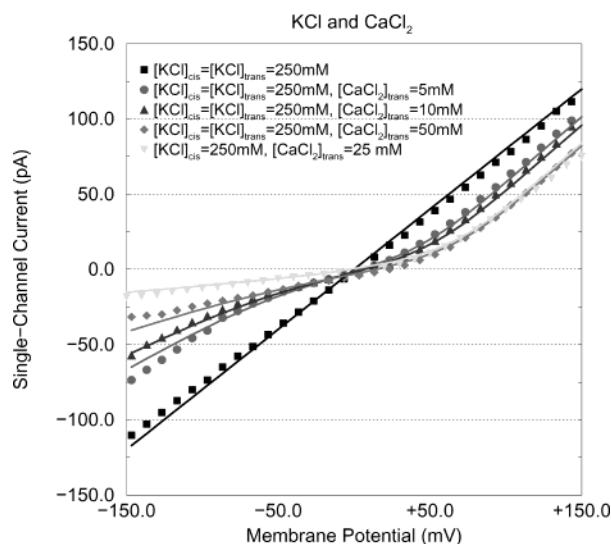


**Figure 1.** Extended PNP fits to current–voltage relations in mixtures of KCl and  $\text{CaCl}_2$ . Single-channel ionic currents were measured in the indicated solutions in the cis and trans chambers of the lipid bilayer setup. The symbols show the experimental data and the lines the PNP fits. The cis and trans solutions contain  $4 \mu\text{M}$   $\text{Ca}^{++}$ , if the concentrations of  $\text{CaCl}_2$  are not explicitly indicated.

## Barrier model, PNP, and experiment

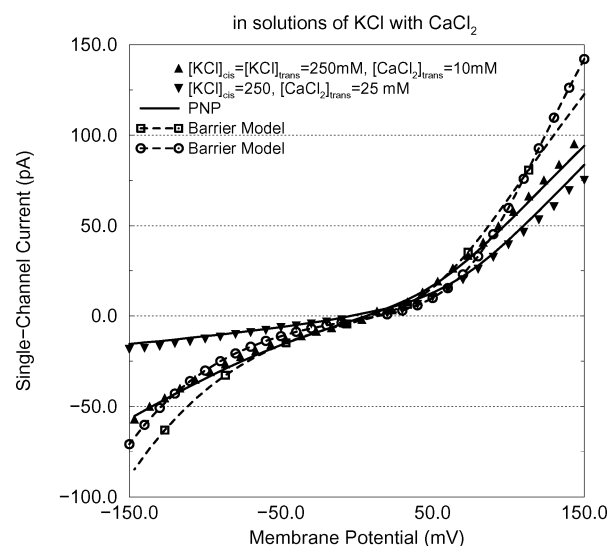


**Figure 2.** Comparison of the fits of the barrier and extended PNP models with experimental data in mixtures of KCl and  $\text{CaCl}_2$ . Single-channel ionic currents were measured in the indicated cis and trans solutions. The solid symbols show the experimental data, the solid lines the extended PNP fits, and the broken lines with the open symbols the barrier model fits.

calcium ion fluxes can be predicted in ionic solutions of any calcium concentration by the extended PNP theory. We make some of these predictions here.

## Results and Conclusions

The 21 current voltage relations—15 measured in symmetrical  $\text{K}^+$  (Figure 1),  $\text{Na}^+$  (not shown), and  $\text{Cs}^+$  (not shown) salts at 0.25 M with various  $\text{Ca}^{++}$  concentrations, along with five more measured in  $\text{K}^+$  solutions containing  $\text{Mg}^{++}$  (Figure 3) and one containing  $\text{Ca}^{++}$  and  $\text{Mg}^{++}$  (Figure 4)—are fitted simultaneously by the extended PNP. All parameters stay the same from solution

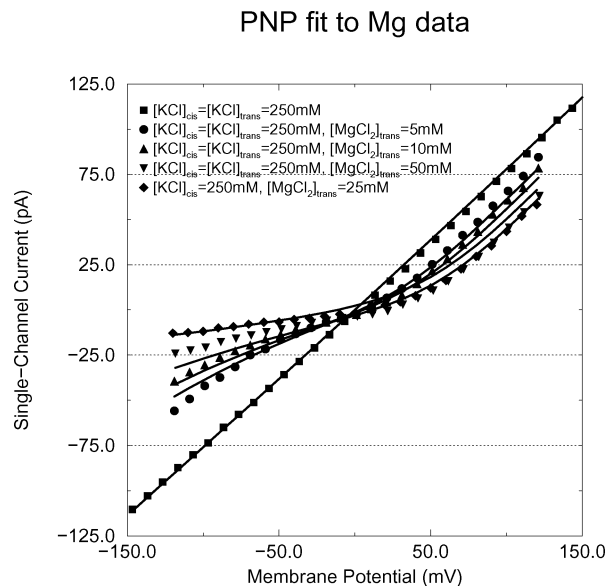


**Figure 3.** Current–voltage relations in mixtures of KCl and  $\text{MgCl}_2$ . Single-channel ionic currents were measured in the indicated cis and trans solutions, both containing  $4 \mu\text{M Ca}^{++}$ . The symbols show the experimental data and the lines the extended PNP fits.

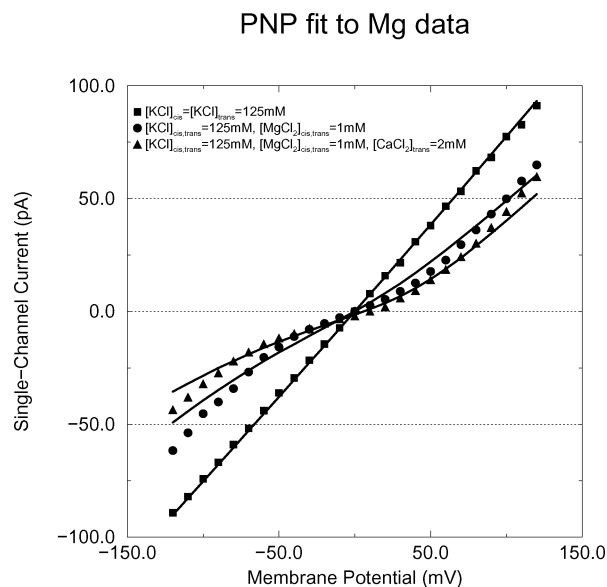


**Figure 4.** Extended PNP fits to current–voltage relations in mixtures of KCl,  $\text{CaCl}_2$ , and  $\text{MgCl}_2$ . Single-channel ionic currents were measured in the indicated cis and trans solutions. The symbols show the experimental data and the solid lines the extended PNP fits. The cis and trans solutions contain  $4 \mu\text{M Ca}^{++}$ , if the concentrations of  $\text{CaCl}_2$  are not explicitly indicated.

to solution and from voltage to voltage. For example, the parameters of  $\text{Cl}^-$  are the same in the calculation of IV's in all twenty-one solutions. The details of the least-squares fit have been described.<sup>1</sup>

The obtained permeation parameters for  $\text{Ca}^{++}$  and  $\text{Mg}^{++}$  are as follows:  $D(\text{Ca}) = 8.4(\pm 0.7) \times 10^{-8} \text{ cm}^2/\text{s}$ ,  $\bar{\mu}(\text{Ca}) = -91(\pm 6) \text{ mV}$ ;  $D(\text{Mg}) = 5.4(\pm 0.7) \times 10^{-8} \text{ cm}^2/\text{s}$ ,  $\bar{\mu}(\text{Mg}) = -53(\pm 6) \text{ mV}$ . For reference,  $D(\text{Ca}) = 1.1 \times 10^{-5}$  in 100 mM  $\text{CaCl}_2$  bulk solution.  $D(\text{Mg})$  in bulk is very similar.

The 21 IV's have a total of 616 measured IV points. The rms current value of the IV points is 40.0 pA ( $I_{\text{rms}} = \sqrt{1/N \sum_i \sum_j I_{ij}^2}$ ,  $j$  denotes each IV point in the same ionic solution,  $i$  denotes different ionic solutions, and  $N$  is the total number of IV-points in all solutions). The rms deviation of the

least-squares fit ( $\sqrt{1/N \sum_i \sum_j (I_{ij}^{\text{PNP}} - I_{ij})^2}$ ) is 2.9 pA, which is equivalent to 7–8% error.

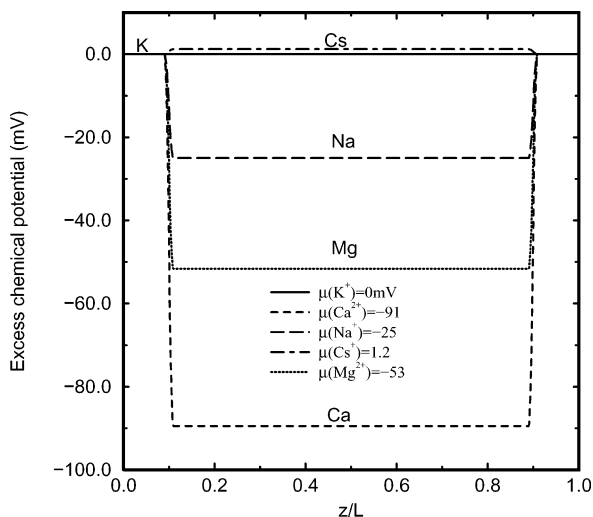
Figure 1 shows the fits to five current voltage curves in symmetric KCl without added trans (SR luminal)  $\text{CaCl}_2$  (squares) and with 5 mM (circles), 10 mM (triangle up), and 50 mM (diamonds)  $\text{CaCl}_2$  added to the trans side of the bilayer, and with 250 mM KCl on the cis side and 25 mM  $\text{CaCl}_2$  on the trans side but without trans KCl (triangle down). The extended PNP—solid lines—fits the experimental data very well, with some deviations at high negative and positive holding potentials. The fits to the corresponding IV relations in the mixtures of NaCl and CsCl with  $\text{CaCl}_2$  are similar to the fits in the KCl solutions (not shown).

Figure 2 compares experimental data in two mixtures of KCl and  $\text{CaCl}_2$  with fits from the extended PNP and the classical barrier model. The fits for the barrier model were calculated using the four barrier and three binding site model of<sup>21</sup> with a prefactor for an ideal gas and a computer program kindly provided by Dr. Alvarez.<sup>29</sup> The up-triangles are IV points measured in symmetrical 250 mM KCl with 10 mM  $\text{CaCl}_2$  on the trans side, and the fit by the barrier model for this ionic solution is the dash line with open squares. The down-triangles are the measured IV points in the bi-ionic solution of 250 mM KCl on the cis side and 25 mM  $\text{CaCl}_2$  on the trans side, and the dash line with open circles is the fit by the barrier model for this ionic solution. The solid lines are the fit from the extended PNP. The PNP model fits the experimental data well at holding potentials ranging from  $-150$  to  $+150$  mV. By comparison, the barrier model failed to fit the experimental data at holding potentials more negative than  $-50$  mV or more positive than  $50$  mV. Similar fits by the extended PNP formulation and deviations by the barrier model were obtained when these were applied to mixtures of NaCl or CsCl with  $\text{CaCl}_2$  (not shown).

The free  $\text{Mg}^{++}$  concentration in cardiac muscle has been reported to range from 0.7 to 1.0 mM.<sup>30</sup> The extended PNP fits to the current–voltage relations in KCl solutions with  $\text{Mg}^{++}$  present on the trans side are shown in Figure 3. The experimental data are well fit by the extended PNP formation at holding potentials from  $-50$  to  $+50$  mV. At higher voltages, the fits deviate from the data in symmetric KCl solutions containing 5 and 50 mM  $\text{MgCl}_2$ . The extended PNP fits well the experimental data in the bi-ionic solution containing 250 mM cis KCl and 25 mM trans  $\text{MgCl}_2$  at positive but not at negative holding potentials. Figure 4 shows the extended PNP fits to the current–voltage relations to symmetric 125 mM KCl and 1 mM  $\text{MgCl}_2$  solutions without (circles) and with (triangles) 2 mM  $\text{Ca}^{++}$  on the trans-side. The data are fit well with some deviations observed beyond the  $-75$  to  $+75$  mV range.

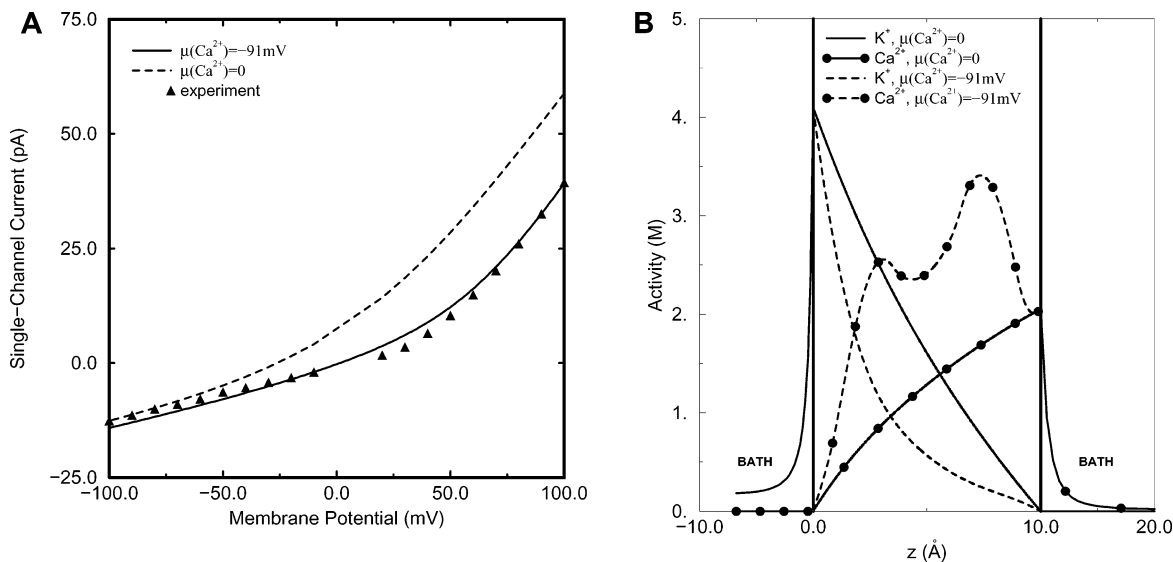
Figure 5 shows the excess chemical potentials for the cations used in fitting the data in Figures 1–4 as well as those in mixtures of NaCl or CsCl with  $\text{Ca}^{++}$ . The data for the monovalent cations are taken from ref 1. The excess chemical potential of  $-91$  mV for  $\text{Ca}^{++}$  and  $-53$  mV for  $\text{Mg}^{++}$  are determined from the data of the present study. The values of excess chemical potentials are assigned from 1 to 9 Å in the selectivity filter region (the entire region is 10 Å). No attempt was made to vary the length of the region of the excess chemical potential profiles, because the exact location has been shown to be unimportant.<sup>1</sup>

Figure 6 shows the effects of the excess chemical potential on the fits of voltage-dependence of single-channel  $\text{Ca}^{++}$  currents and the distribution of  $\text{Ca}^{++}$  within the channel selectivity filter. Data are shown for a bi-ionic solution of 250



**Figure 5.** Excess chemical potentials used in the extended PNP calculations. The excess chemical potentials for  $\text{Ca}^{2+}$  and  $\text{Mg}^{2+}$  are obtained from least-square fits. The values of the monovalent cations are taken from 1. In the calculations, the 10 Å pore region from 1 to 9 Å is assigned a different excess chemical potential than the bulk solution, where it is zero. In the calculation, the exact region assigned with the value of excess chemical potential is not critical and will only affect the numerical values.

mM KCl at the cis side and 25 mM  $\text{CaCl}_2$  at the trans side of the bilayer. Figure 6A compares experimental data with two predicted IV curves obtained with  $\bar{\mu}(\text{Ca}) = -91$  mV or  $\bar{\mu}(\text{Ca}) = 0$ . Strong “binding” of  $\text{Ca}^{2+}$  to the RyR2 pore is necessary to match the measured and predicted IV curves. Even though the experimental data fit reasonably well the predicted curve assuming strong  $\text{Ca}^{2+}$  binding, the reversal potential was offset by 5.4 mV (1.5 mV as compared to a measured reversal



**Figure 6.** (A) Predicted current voltage relations in the absence and presence of an excess chemical potential. The predicted IV relations with 250 mM KCl at the cis side and 25 mM  $\text{CaCl}_2$  at the trans side. Triangles are the experimental data. Solid line is the IV relation calculated with  $\bar{\mu}(\text{Ca}) = -91$  mV, and the broken line is predicted by the extended PNP when  $\bar{\mu}(\text{Ca}) = 0$  mV. The data show that it is necessary to have a strong chemical interaction of  $\text{Ca}^{2+}$  with the RyR2 pore to fit the data. Note  $D(\text{K}) = 1.1 \times 10^{-6}$  cm<sup>2</sup>/s is used in this figure. (B) Predicted activity profiles in the absence and presence of an excess chemical potential. The activity profiles of  $\text{Ca}^{2+}$  and  $\text{K}^+$  in the same bionic solution as that in panel A, without (solid lines) and with (broken lines) a chemical interaction of  $\text{Ca}^{2+}$  with RyR2, at applied membrane potential of 0 mV. The solid line is the activity profile of the  $\text{K}^+$  in the absence of  $\text{Ca}^{2+}$  chemical interaction with RyR2. It rises due to the surface Donnan potential from the cis bath. Inside the pore, it has the profile of a nearly linear gradient from cis side (left) to zero concentration (right). This is the case of simple diffusion from a high to zero concentration, with a small nonlinear effect from the interaction of  $\text{Ca}^{2+}$  with the permanent charge along the RyR2 pore. A similar  $\text{Ca}^{2+}$  activity profile is obtained when there is no chemical interaction (solid line with filled circles). It rises from the trans side bath, follows a nearly linear line, and falls to zero on the cis side bath. The situation is very different when there is a strong chemical interaction of  $\text{Ca}^{2+}$  with the RyR2 pore, described by an excess chemical potential of  $-91$  mV. The strong binding of  $\text{Ca}^{2+}$  elevates the activity of  $\text{Ca}^{2+}$  (dash line with filled circles) to a higher concentration than when there is no binding in the pore (solid line with filled circles).

potential of 6.9 mV; the experimental IV relation is fit by a cubic spline, and then the reversal potential is found with the fit spline). No attempt was made to correct this discrepancy, because it would require that the weight of the least-squares fits near the reversal potential be enhanced.

Figure 6B plots the activity profiles of  $\text{Ca}^{2+}$  and  $\text{K}^+$  at an applied transmembrane potential of 0 mV. Comparison of the dash and solid lines with the solid circles shows that, as a consequence of strong binding, the activity (concentration) of  $\text{Ca}^{2+}$  is elevated in the binding region (assumed to range from 1 to 9 Å in Figure 6B) of the 10 Å long selectivity filter. The two peaks in the  $\text{Ca}^{2+}$  activity profile (dash line with solid circles) are the direct consequence of jumps in the excess chemical potentials at 1 and 9 Å (Figure 5, where it is assumed that excess chemical potential is a step function and it only has two discontinuities from bulk from each side. More complicated functional shape of excess chemical potential will introduce more free parameters, and it is not used in present study). They reflect an attractive local chemical interaction of  $\text{Ca}^{2+}$  with the selectivity filter, mimicking the effect of a binding site in the filter region of RyR2. The physical origin of such binding (attractive short-range local interaction) needs to be investigated by a detailed molecular theory, such as the mean-spherical-approximation theory<sup>31</sup> or a detailed molecular dynamic simulation with an appropriate force field, combined with the specific knowledge of the RyR2 structure. The dash line shows the  $\text{K}^+$  activity profile with  $\bar{\mu}(\text{Ca}) = -91$  mV. The  $\text{K}^+$  occupancy is reduced because of electrostatic repulsion when the  $\text{Ca}^{2+}$  occupation is increased, due to a stronger  $\text{Ca}^{2+}$  chemical binding locally. The solid line is the  $\text{K}^+$  activity profile when  $\bar{\mu}(\text{Ca}) = 0$ . A nearly linear profile is calculated from a high potassium ion activity on the cis side (left) to zero activity on the trans side (right). This is a case of simple diffusion from high to zero

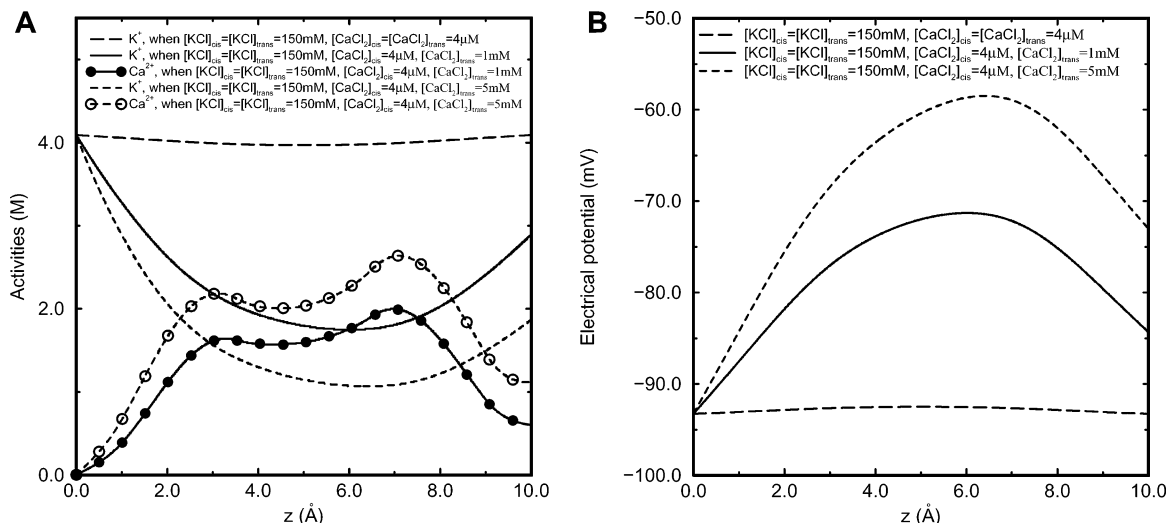


**Figure 7.** (A) Activity profiles in the absence and presence of  $Ca^{++}$ . Shown are the activity profiles of the permeating ions ( $K^+$  and  $Ca^{++}$ ) at zero membrane potential in symmetric 150 mM KCl without added  $CaCl_2$  and with 1 mM and 5 mM  $CaCl_2$  at the trans side. The bath profiles are omitted for clarity. The profiles for  $Cl^-$  are omitted because they are negligible. The dash and solid lines without symbols are for  $K^+$  (long-dash line without  $Ca^{++}$  ions; solid line with 1 mM  $Ca^{++}$ ; short-dash with 5 mM  $Ca^{++}$ ). The solid line with filled circles is for 1 mM  $Ca^{++}$  trans, and the dash line with the open circles is for 5 mM  $Ca^{++}$  trans. The profiles show that  $Ca^{++}$  strongly competes with  $K^+$  in the RyR2 pore region. (B) Electrical potential profiles in the absence and presence of  $Ca^{++}$ . Shown are the electrical potential profiles for three symmetric 150 mM KCl solutions without added  $CaCl_2$  (long-dash lines) and with 1 mM (solid line) and 5 mM (short-dash line)  $CaCl_2$  added to at trans side.

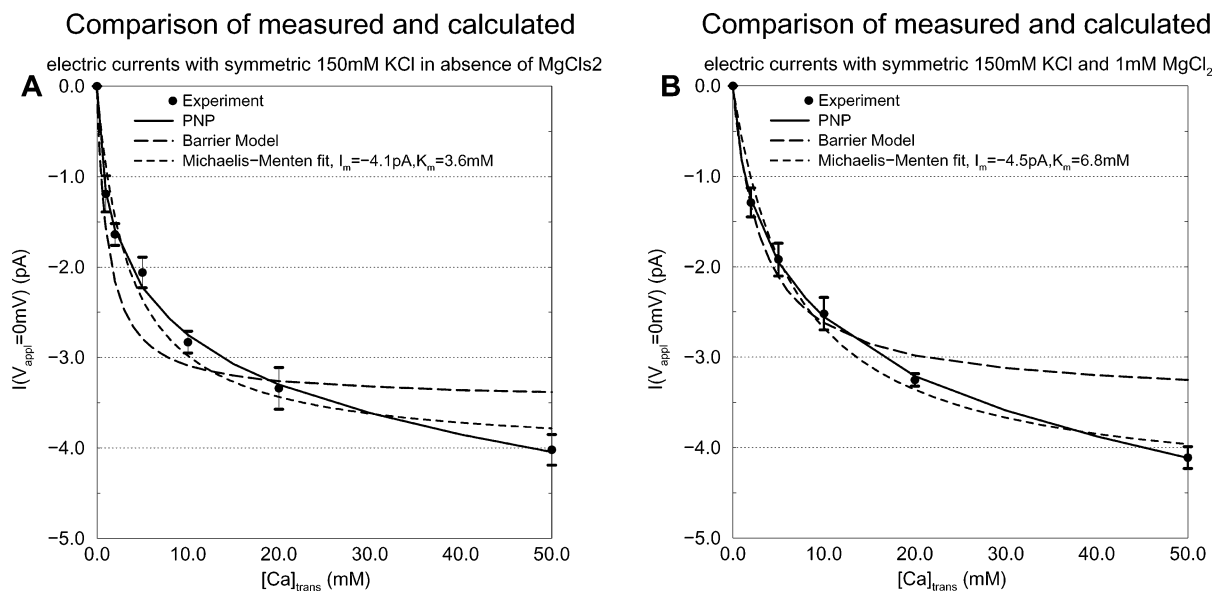


**Figure 8.** (A) Comparison of predicted and measured electric currents at zero applied membrane potentials. Ionic currents are measured in symmetric 150 mM KCl in the absence of symmetric 1 mM  $MgCl_2$  and the indicated concentrations of trans  $CaCl_2$ . Solid points indicate the experimental data, and the solid line is predicted by the extended PNP and the long-dash lines by the barrier model. The short-dash line was obtained assuming single site kinetics as described by the Michaelis-Menten equation. Experimental data are the mean  $\pm$  S.E. of 4–5 experiments. (B) As Figure 8A but the presence of 1 mM symmetric  $MgCl_2$ . Experimental data are the mean  $\pm$  S.E. of 3 experiments.

concentration. The small nonlinear effect arises from the repulsion of  $K^+$  by  $Ca^{++}$  and from the attraction of  $Ca^{++}$  to the RyR2 pore. (The curve would have been linear in the absence of calcium ions because it would be a case of a simple self-diffusion.) When  $\bar{\mu}(Ca) = 0$ , the potassium ion occupancy ( $O_{K^+} = \pi r^2 N_A \int_0^L C(K^+, \zeta) d\zeta$ , where  $N_A$  is Avogadro's number and  $L$  is the length of the channel) is 0.4. The occupancy of  $Ca^{++}$  is 0.28. The two kinds of cations together neutralize the overall charge in the pore region if the electrostatic interaction is the only interaction. When  $\bar{\mu}(Ca) = -91$  mV, however, an extra short-range local chemical interaction must be included. In this case, the potassium ion occupancy is 0.2 (reduced because of the preference in  $Ca^{++}$  binding) and  $Ca^{++}$  occupancy increases to 0.5. Note that overall charge neutrality is violated because of the extra short-range local chemical interaction,

which can introduce extra energy to accommodate such deviation from charge neutrality.

The SR membrane is freely permeable to monovalent ions,<sup>32</sup> which suggests a SR membrane potential near zero. Figure 7 shows the predicted activity profiles and electrical potential profiles in two ionic solutions of physiological interest at an applied transmembrane voltage of 0 mV. The two solutions are symmetrical 150 mM KCl with 1 mM  $CaCl_2$  and with 5 mM  $CaCl_2$  added to the trans side, compared to the case in a symmetrical 150 mM KCl without added  $CaCl_2$ . Figure 7A shows the activity profiles of  $K^+$  and  $Ca^{++}$ . The profiles for  $Cl^-$  are omitted because they are negligible. The long-dash line is the  $K^+$  activity profile in the symmetrical 150 mM KCl solution without added  $Ca^{++}$ . The solid and short-dash lines are for  $K^+$  with 1 mM and 5 mM  $CaCl_2$  at the trans side, respectively, and

the lines with the circles are for  $\text{Ca}^{++}$ . The profiles show that 1 mM (solid line) and 5 mM (short-dash line)  $\text{Ca}^{++}$  strongly compete with  $\text{K}^{+}$  to occupy the selectivity filter region of RyR2 channel pore. The occupancy of  $\text{K}^{+}$  is significantly reduced by  $\text{Ca}^{++}$ , when the calcium ion concentration in the trans side is raised from 1 mM to 5 mM (solid vs short dash line). Figure 7B compares the electrical potential profiles for the above three conditions. The long-dash lines is for  $\text{K}^{+}$  without added  $\text{Ca}^{++}$ , and the solid-line and short-dash line are for 1 and 5 mM  $\text{Ca}^{++}$  in the trans bath, respectively. Occupancy by  $\text{Ca}^{++}$  raises the electrical potential in the RyR2 selectivity filter region to less negative values.

Figure 8 compares  $\text{Ca}^{++}$  currents measured at zero applied membrane potential with those calculated by the extended PNP and barrier models. Figure 8A shows the effects of increasing  $\text{Ca}^{++}$  concentrations on the electrical currents in symmetric 150 mM KCl solution with trans  $\text{Ca}^{++}$  concentrations ranging from 1 to 50 mM. In Figure 8B, the same measurements were performed in the presence of symmetric 1 mM  $\text{Mg}^{++}$ . In both cases the currents follow single site kinetics as described by the Michaelis–Menten equation, giving maximal currents of 4.1 and 4.5 pA for the 0 mM (Figure 8A) and 1 mM (Figure 8B)  $\text{Mg}^{++}$  solutions, respectively. The respective  $\text{Ca}^{++}$  concentrations for half-maximal  $\text{Ca}^{++}$  currents are 3.6 and 6.8 mM, indicating that  $\text{Mg}^{++}$  ions compete with  $\text{Ca}^{++}$  ions in the selectivity filter. Figure 8A,B further shows that the extended PNP formulation predicts well the calcium ion currents at 0 mV, i.e., the membrane potential of SR in muscle. The barrier model fit the experimental data less well. The model overestimates the  $\text{Ca}^{++}$  currents at low  $[\text{Ca}^{++}]$  in the absence of  $\text{Mg}^{++}$  and underestimates the  $\text{Ca}^{++}$  currents at high  $[\text{Ca}^{++}]$  both in the absence and presence of 1 mM  $\text{Mg}^{++}$ .

Taken together, the results of Figures 1–8 demonstrate that the extended PNP formulation of electrodiffusion is capable of fitting a vast range of experimental data simultaneously. Input parameters to the extended PNP theory are the channel protein geometry and charge distribution, the dielectric properties of the lipid membrane and channel protein, and the ion diffusion coefficients. Outputs are the ion currents and their concentration and voltage dependence. Some input parameters such as the dielectric constants of the pore and lipid membrane are assigned to the values in the bulk. We assessed their contribution to the fitting parameters by changing them within a reasonable range. For example, a change in the dielectric constant of the channel pore from 80 to 20 in the computer numerical simulation does not significantly change the fitting parameters. A detailed molecular simulation of the channel physical parameters requires that the molecular structure of the pore is known.

In conclusion, the extended PNP provides an estimation of the RyR2 ion diffusion constants and electrostatic interactions in a self-consistent coherent formulation. Its predictive power was tested by calculating the  $\text{Ca}^{++}$  currents as a function of

SR lumenal  $\text{Ca}^{++}$  concentration. The results show that the extended PNP formulation accurately predicts the  $\text{Ca}^{++}$  currents under physiological relevant conditions and thus can provide important information on the function of the RyR2.

**Note Added after ASAP Posting.** This article was posted ASAP on 7/26/2003. Several changes have been made to the text, including changing a reference on page 5 from Figure 6A to Figure 5. The correct version was posted on 7/31/2003.

## References and Notes

- (1) Chen, D. P.; Xu, L.; Tripathy, A.; Meissner, G.; Eisenberg, B. *Biophys. J.* **1999**, *76*, 1346.
- (2) Coronado, R.; Morrissette, J.; Sukhareva, M.; Vaughan, D. M. *Am. J. Physiol.* **1994**, *266*, C1485.
- (3) Meissner, G. *Annu. Rev. Physiol.* **1994**, *56*, 485.
- (4) Franzini-Armstrong, C.; Protasi, F. *Physiol. Rev.* **1997**, *77*, 699.
- (5) Samsó, M.; Wagenknecht, T. *Struct. Biol.* **1998**, *98*, 172.
- (6) Takeshima, H.; Nishimura, S.; Matsumoto, T.; Ishida, H.; Kangawa, K.; Minamino, N.; Matsuo, H.; Ueda, M.; Hanaoka, M.; Hirose, T.; Numa, S. *Nature* **1989**, *339*, 439.
- (7) Zorzato, F.; Fujii, J.; Otsu, K.; Phillips, M.; Green, N.; Lai, F.; Meissner, G.; MacLennan, D. *J. Biol. Chem.* **1990**, *65*, 2244.
- (8) Grunwald, R.; Meissner, G. *J. Biol. Chem.* **1995**, *270*, 11338.
- (9) Wang, J.; Needleman, D.; Seryshev, A.; Aghdasi, B.; Slavik, K.; Liu, S.; Pedersen, S.; Hamilton, S. *J. Biol. Chem.* **1996**, *271*, 8387.
- (10) Bhat, M.; Zhao, J.; H, T.; J., M. *Biophys. J.* **1997**, *73*, 1329.
- (11) Sitsapesan, R.; Montgomery, R.; Williams, A. *Circ. Res.* **1995**, *77*, 765.
- (12) Gyorke, I.; Gyorke, S. *Biophys. J.* **1998**, *75*, 2801.
- (13) Tripathy, A.; Meissner, G. *Biophys. J.* **1996**, *70*, 2600.
- (14) Xu, L.; Meissner, G. *Biophys. J.* **1998**, *75*, 2302.
- (15) Smith, J.; Coronado, R.; Meissner, G. *Nature* **1985**, *316*, 446.
- (16) Rousseau, E.; Smith, J.; Henderson, J.; Meissner, G. *Biophys. J.* **1986**, *50*, 1009.
- (17) Lai, F.; Erickson, H.; Rousseau, E.; Liu, Q.; Meissner, G. *Nature* **1988**, *331*, 315.
- (18) Smith, J.; Imagawa, T.; Ma, J.; Fill, M.; Campbell, K.; Coronado, R. *J. Gen. Physiol.* **1988**, *92*, 1.
- (19) Lindsay, A. R. G.; Manning, S. D.; Williams, A. J. *J. Physiol.* **1991**, *439*, 463.
- (20) Liu, Q.-Y.; Lai, A.; Rousseau, E.; Jones, R. V.; Meissner, G. *Biophys. J.* **1989**, *55*, 415.
- (21) Tinker, A.; Linday, A. R. G.; Williams, A. J. *J. Gen. Physiol.* **1992**, *100*, 495.
- (22) Chen, D. P.; Xu, L.; Tripathy, A.; Meissner, G.; Eisenberg, B. *Biophys. J.* **1997**, *73*, 1337.
- (23) Lee, H.; Xu, L.; Meissner, G. *J. Biol. Chem.* **1994**, *269*, 13305.
- (24) Chen, D. P. Nonequilibrium Thermodynamics of Transports in Ion Channels. In *Progress of Cell Research: Towards Molecular Biophysics of Ion Channels*; Sokabe, M., Auerbach, A., Sigworth, F., Eds.; Elsevier Science: Amsterdam, 1997; Volume 6, pp 269–277.
- (25) Chen, D. P.; Eisenberg, R. S. *Biophys. J.* **1993**, *64*, 1405.
- (26) Selberherr, S. *Analysis and Simulation of Semiconductor Devices*; Springer-Verlag: Vienna, 1984.
- (27) Green, W. N.; Andersen, O. S. *Annu. Rev. Physiol.* **1991**, *53*, 341.
- (28) Robinson, R. A.; Stokes, R. H. *Electrolyte Solutions*, 2nd ed.; Butterworth: London, 1959.
- (29) Alvarez, O.; Villaroel, A.; Eisenman, G. *Methods Enzymol.* **1992**, *207*, 816.
- (30) Murphy, E.; Steenbergen, C.; Levy, L. A.; Raju, B.; London, R. E. *J. Biol. Chem.* **1989**, *264*, 5622.
- (31) Durand-Vidal, S.; Turq, P.; Bernard, O.; Treiner, C.; Blum, L. *Physica A* **1996**, *231*, 123.
- (32) Meissner, G. *Mol. Cell. Biochem.* **1983**, *55*, 65.